Bilayer stacking *A*-type altermagnet: A general approach to generating two-dimensional altermagnetism

Sike Zeng and Yu-Jun Zhao*

Department of Physics, South China University of Technology, Guangzhou 510640, China

(Received 22 July 2024; accepted 9 October 2024; published 6 November 2024)

In this paper, we propose a concept of bilayer stacking *A*-type altermagnet (BSAA), in which two identical ferromagnetic monolayers are stacked with antiferromagnetic coupling to form a two-dimensional (2D) *A*-type altermagnet. By solving the stacking model, we derive all BSAAs for all layer groups and draw three key conclusions: (i) Only 17 layer groups can realize intrinsic *A*-type altermagnetism. All 2D *A*-type altermagnets must belong to these 17 layer groups, which will be helpful to search for 2D *A*-type altermagnet. (ii) It is impossible to connect the two sublattices of BSAA using S_{3z} or S_{6z}, a constraint that is also applicable to all 2D altermagnets. (iii) $C_{2\alpha}$ is a general stacking operation to generate BSAA for an arbitrary monolayer. Our theory not only can explain the previously reported twisted-bilayer altermagnets, but also can provide more possibilities to generate *A*-type altermagnets. Our research has significantly broadened the range of candidate materials for 2D altermagnets. Based on conclusion (i), the bilayer $NiZrCl_6$ is predicted to exhibit intrinsic *A*-type altermagnetism. Additionally, we use twisted-bilayer $NiCl_2$ and CrOCl as supplementary examples of BSAA. Furthermore, utilizing symmetry analysis and first-principles calculation, we scrutinize their spin-momentum locking characteristic to substantiate their altermagnetic properties.

DOI: 10.1103/PhysRevB.110.174410

I. INTRODUCTION

Recently, altermagnetism has garnered significant attention in condensed matter physics [1–11], due to its fascinating physical properties and potential applications in the spintronics. Initially proposed in several scientific literature [12–16] and later formalized under the term "altermagnetism" [17], this phenomenon has emerged as the third magnetic state within the context of spin group [17,18]. Altermagnetism is distinguished by collinear-compensated magnetic order in real space, like antiferromagnetism, and the breaking of time-reversal symmetry in reciprocal space, like ferromagnetism. Unlike antiferromagnets, altermagnets are characterized by the connection of opposite sublattices via proper or improper rotation, rather than translation or inversion symmetry, which results in the disruption of *PT* symmetry [17]. Recent experiments have reported spin-splitting electronic structure in the altermagnet, utilizing angle-resolved photoemission spectroscopy, which offers direct evidence for altermagnetism [19,20].

From an application perspective, altermagnets present considerable potential for applications in the spintronics, due to their advantageous properties, such as the absence of stray field, THz spin dynamics, and strong time-reversal symmetry breaking. It has been suggested that giant and tunneling magnetoresistance (GMR and TMR) effect [21] can be generated in altermagnets. Moreover, as a new type of torque, spin-splitter torque (SST), combining the advantage of spin-transfer torque (STT) and spin-orbit torque (SOT), has been reported in the altermagnet theoretically [22] and experimentally [23,24]. As is known to all, two-dimensional (2D) materials are sensitive to external stimuli than thin films, which allows their properties to be efficiently controlled. In addition, 2D materials can be easily stacked with each other to form heterostructures with different properties. Two-dimensional altermagnets possess all of the aforementioned features, so we think that 2D altermagnets will be useful in the spintronics.

To date, a multitude of three-dimensional (3D) altermagnets have been identified [3]. However, two-dimensional intrinsic altermagnets were rarely reported [25,26]. The expansion of two-dimensional materials exhibiting altermagnetism will greatly enhance our understanding of the fundamental properties of altermagnets and promote their applications in the spintronics. Therefore, significant efforts have been devoted to enriching the candidate materials for 2D altermagnet [27–31].

In 2D systems, the spin degeneracy of the nonrelativistic band structure for all **k** vectors in the whole Brillouin zone is protected by four spin-group symmetries [26]. The spin-group symmetry is denoted as $[R_i||R_j]$, where the transformations on the left of the double bar only act on the spin space and those on the right of the double bar only act on the real space. For all 2D systems mentioned in this paper, it is assumed that they lie parallel to the *xy* plane. First, $[C_2||\tau]$ symmetry, where C_2 represents twofold rotation around an axis perpendicular to the spins and τ represents translation symmetry connecting atoms of the opposite sublattices, results in the spin-degeneracy band structure. Moreover, the spin degeneracy is also protected by $[C_2||\overline{E}]$, in which $\overline{E}$ represents inversion symmetry. Its physical signification is that the atoms of the opposite sublattices

*Contact author: zhaoyj@scut.edu.cn

are connected by inversion symmetry. The aforementioned symmetries also maintain band structure spin degeneracy in 3D systems. However, compared to 3D systems, there are two extra symmetries to protect spin degeneracy in 2D systems. One is $[C_2||m_z]$, which represents that the atoms of the opposite sublattices can be connected by the mirror symmetry through the xy plane. The other is $[C_2||C_{2z}]$, which represents the atoms of the opposite sublattices can be connected by a twofold rotation around the z axis.

Based on the above discussion, we can conclude the requirements for the emergence of altermagnetism in 2D materials: (i) The system must exhibit collinear-compensated magnetic order, i.e., it must have two sublattices with antiparallel magnetic moments. (ii) The atoms of the opposite sublattices cannot be connected by translation symmetry, inversion symmetry, mirror symmetry through the xy plane or a twofold rotation around the z axis, given that the system is parallel to the xy plane. (iii) There must exist at least one symmetry operation that interconnects the opposite sublattices, which can be proper or improper rotation. Therefore, we can discern that the emergence of 2D altermagnetism entails more requirements on symmetry, which may be why 2D intrinsic altermagnets were rarely reported.

In 2D systems, translational symmetry is inherently absent in the out-of-plane direction, which serves as the foundation for this work. A-type altermagnetism involves a bilayer system that can be considered as comprising two single ferromagnetic layers. In this system, the bottom layer remains stationary, while the top layer is stacked on top with antiferromagnetic coupling. We notice that A-type altermagnets, which exhibit intralayer ferromagnetic coupling and interlayer antiferromagnetic coupling, inherently satisfy the requirement that the opposite sublattices cannot be connected by translation symmetry and a twofold rotation around the z axis. Therefore, we believe that A-type altermagnetism is easier to appear in 2D materials.

Here, we propose a concept of bilayer stacking A-type altermagnet (BSAA). Utilizing the stacking model, we have solved for all BSAAs, as listed in Table I. Interestingly, based on the solutions, we draw three intriguing conclusions in Sec. II. To facilitate further research on BSAA, we classify all BSAAs using spin layer group, as listed in Table II. Moreover, we predict that bilayer $NiZrCl_6$ exhibits intrinsic A-type altermagnetism in Sec. III, which has never been reported previously. In addition, we notice that twisted-bilayer A-type altermagnets reported in the previous works [30,31] are encompassed within BSAAs and can be understood using this theory, as twisting can be regarded as a stacking operation. Therefore, we use twisted-bilayer $NiCl_2$ [30] and CrOCl as supplementary examples of BSAA in Sec. IV. Finally, to illustrate the universality of BSAA, we have identified materials, reported in the relevant studies [30–32], as BSAAs in Sec. V. Of course, these examples are just the beginning of BSAA. We believe that there is a vast range of BSAA. As Table I presents, a diverse set of stacking operations can generate BSAA.

II. ALL POSSIBILITIES OF BILAYER STACKING *A*-TYPE ALTERMAGNETS

We now focus on the derivation of all BSAAs for all layer groups, where two identical ferromagnetic monolayers are stacked with antiferromagnetic coupling to form a two-dimensional A-type altermagnet. Employing different stacking configurations, a specific monolayer can form bilayers with different symmetries. As a result, some stacking configurations can generate A-type altermagnetism for a specific ferromagnetic monolayer, while others can not.

First, we introduce the model for BSAA. The model is based on the sole assumption of intralayer ferromagnetic coupling and interlayer antiferromagnetic coupling, which satisfies the requirement (i) of forming 2D altermagnetism. Due to the nonrelativistic nature of altermagnetism, real space and spin space are independent of each other. Therefore, we focus only on real-space transformations, i.e., space-group symmetries, because of the above assumption. Meanwhile, we find that two remaining requirements, requirements (ii) and (iii), are solely related to the symmetry operations that interconnect two sublattices. Consequently, we are primarily concerned with the symmetry operations that exchange the positions of the two ferromagnetic layers.

All 2D point-group symmetry operations can be summarized into seven types [33]: (i) identity E; (ii) inversion $\overline{E}$; (iii) mirror symmetry through the xy plane m_z; (iv) mirror symmetry m_α is perpendicular to the xy plane and parallel to the direction $[\cos(\alpha), \sin(\alpha), 0]$; (v) n-fold rotation symmetry along the z axis C_{nz}; (vi) twofold rotation symmetry $C_{2\alpha}$ along the direction $[\cos(\alpha), \sin(\alpha), 0]$; (vii) n-fold rotation symmetry with mirror symmetry along the z axis S_{nz}. According to whether they reverse the z coordination, they can further be classified into two categories R^+ and R^-. R^- can reverse the z coordination, while R^+ can not. R^- contains $\{\overline{E}, m_z, C_{2\alpha}, S_{nz}\}$, and R^+ contains $\{E, C_{nz}, m_\alpha\}$. In the context of this paper, R^- represents the symmetry operations that exchange the positions of the two ferromagnetic layers, while R^+ does not. Therefore, we conclude that to obtain all BSAAs for all layer groups, it is sufficient to calculate all stacking operations generating R^- in the bilayer for each layer group. Subsequently, we exclude the stacking operations generating $\{\overline{E}, m_z\}$ in the bilayer from those generating $\{C_{2\alpha}, S_{nz}\}$ in the bilayer for each layer group. This ensures that two single layers cannot be connected by $\overline{E}$ or m_z, but can be connected by $C_{2\alpha}$ or S_{nz}. Finally, the remaining stacking operations are all the possible operations to generate BSAA from a ferromagnetic monolayer.

Let us assume that the single ferromagnetic layer S, with layer group $G_s = \{\hat{R}_s\}$, is parallel to the xy plane. In this paper, symbols with a caret represent space-group symmetry, while those without a caret represent point-group symmetry. For example, $\hat{R}_s$ represents the space-group symmetry of layer S, while R_s represents the point-group symmetry. The second ferromagnetic layer S' is generated by applying the stacking operation $\hat{\tau}_z\hat{O}$ on S, where $\hat{\tau}_z$ is an arbitrary trivial translation

TABLE I. All stacking operations that can construct BSAA from a ferromagnetic monolayer. The layer groups of the monolayer are listed in the first column. The point-group part of stacking operations for each group is listed in the second column. The third column lists the symmetry exchanging two ferromagnetic layers in the bilayer under the stacking operation listed in the second column. The translation part of stacking operations τ_o is dependent on the interlayer symmetry and τ_s. For $C_{2\alpha}$, translation of arbitrary length perpendicular to the vector $[\cos(\alpha), \sin(\alpha), 0]$, as well as translations by half of the lattice vector in the direction of vector $[\cos(\alpha), \sin(\alpha), 0]$, and their combinations, are all permitted. For S_{4z}, the translation operation should satisfy Eq. (17), (19), and (21). In some cases, certain translations are forbidden, which have been listed in the second column. The symbols E, C, m, S represent identity, rotation, mirror, and rotation with mirror operation, respectively. The plus (+) and minus (−) denote the counterclockwise and clockwise rotations, respectively. The angle in the upper right corner of S_z and C_z represents the rotation angle. The angle in the upper right corner of C_2 and α represent the angle relative to the x axis. The range of α is from 0 to π. $G = (0, 0), A = (\frac{1}{2}, 0), B = (0, \frac{1}{2}), C = (\frac{1}{2}, \frac{1}{2}), G' = (\frac{1}{4}, \frac{1}{4}), A' = (\frac{3}{4}, \frac{1}{4}), B' = (\frac{1}{4}, \frac{3}{4}), G' = (\frac{3}{4}, \frac{3}{4}), M = (\frac{1}{3}, \frac{2}{3}), N = (\frac{2}{3}, \frac{1}{3})$, employing lattice vectors as basis vectors.

Layer group	Point-group part of stacking operation	Interlayer symmetry
1,49,65	$C_{2\alpha}$	$C_{2\alpha}$
2	$C_{2\alpha}, m_{(\alpha-\frac{\pi}{2})}$	$C_{2\alpha}$
3	$C_{2\alpha}$	$C_{2\alpha}$
	S_{4z}^{+}, S_{4z}^{-}	S_{4z}
4-5,51-52,66,74	$C_{2\alpha}, m_{\alpha}$	$C_{2\alpha}$
6-7	$C_{2\alpha}, m_{\alpha}$	$C_{2\alpha}$
	$S_{4z}^{+}, S_{4z}^{-}, C_{4z}^{+}, C_{4z}^{-}$	S_{4z}
8–10,53-54,68	$C_{2\alpha}, C_z^{2\alpha}$	$C_{2\alpha}$
11–13	$C_{2\alpha}, S_z^{2(\alpha-\frac{\pi}{2})}(\alpha \neq 0;\ \tau_o \notin \{G, A, B, C\}(\{G, A, B, C, G', A', B', C'\} for\ 13)$ when $\alpha = \frac{\pi}{2})$	$C_{2\alpha}$
14–18	$C_{2\alpha}, C_z^{2\alpha}, m_{(\alpha+\frac{\pi}{2})}, S_z^{2(\alpha-\frac{\pi}{2})}$	$C_{2\alpha}$
	$(\alpha \neq 0;\ \tau_o \notin \{G, A, B, C\}(\{G, A, B, C, G', A', B', C'\} for\ 18)$ when $\alpha = \frac{\pi}{2})$	
19–22	$C_{2\alpha}, C_z^{2\alpha}$	$C_{2\alpha}$
	$S_{4z}^{+}, S_{4z}^{-}, m_{\frac{3\pi}{4}}, m_{\frac{\pi}{4}}$	S_{4z}
23–26	$C_{2\alpha}, S_z^{2\alpha}(\alpha \neq 0, \frac{\pi}{2})$	$C_{2\alpha}$
	$S_{4z}^{+}, S_{4z}^{-}, C_2^{\frac{3\pi}{4}}, C_2^{\frac{\pi}{4}}$	S_{4z}
27–36	$C_{2\alpha}, C_z^{2(\alpha-\frac{\pi}{2})}, S_z^{2(\alpha-\frac{\pi}{2})}, m_{\alpha}$	$C_{2\alpha}$
	$(\alpha \neq 0;\ \tau_o \notin \{G, A, B, C\}(\{G, A, B, C, G', A', B', C'\} for\ 35-36)$ when $\alpha = \frac{\pi}{2})$	
37–48	$C_{2\alpha}, C_z^{2\alpha}, m_{\alpha}, S_z^{2\alpha}(\alpha \neq 0, \frac{\pi}{2})$	$C_{2\alpha}$
	$S_{4z}^{+}, S_{4z}^{-}, C_{4z}^{+}, C_{4z}^{-}, m_{\frac{3\pi}{4}}, m_{\frac{\pi}{4}}, C_2^{\frac{3\pi}{4}}, C_2^{\frac{\pi}{4}}$	S_{4z}
50	$C_{2\alpha}, m_{(\alpha+\frac{\pi}{4})}$	$C_{2\alpha}$
	$E, C_{2z}, S_{4z}^{+}, S_{4z}^{-}$	S_{4z}
55–56	$C_{2\alpha}, S_z^{2\alpha}(\alpha \neq 0, \pm\frac{\pi}{4}, \frac{\pi}{2})$	$C_{2\alpha}$
57-58	$C_{2\alpha}, m_{(\alpha+\frac{\pi}{4})}, C_z^{2\alpha}, S_z^{2(\alpha+\frac{\pi}{4})}(\alpha \neq \pm\frac{\pi}{4})$	$C_{2\alpha}$
	$E, C_{2z}, S_{4z}^{+}, S_{4z}^{-}, C_{2x}, C_{2y}, m_{110}, m_{1\bar{1}0}$	S_{4z}
59-60	$C_{2\alpha}, m_{(\alpha+\frac{\pi}{4})}, S_z^{2\alpha}, C_z^{2(\alpha-\frac{\pi}{4})}(\alpha \neq 0, \frac{\pi}{2})$	$C_{2\alpha}$
	$E, C_{2z}, S_{4z}^{+}, S_{4z}^{-}, C_2^{110}, C_2^{1\bar{1}0}, m_x, m_y$	S_{4z}
61–64	$C_{2\alpha}, S_z^{2\alpha}, C_z^{2\alpha}, m_{\alpha}(\alpha \neq 0, \pm\frac{\pi}{4}, \frac{\pi}{2})$	$C_{2\alpha}$
67	$C_{2\alpha}, C_z^{2(\alpha-\frac{\pi}{2})}$	$C_{2\alpha}$
69	$C_{2\alpha}, S_z^{2(\alpha-\frac{\pi}{2})}(\alpha \neq 0, \pm\frac{\pi}{3};\ \tau_o \notin \{G, A, B, C\}$ when $\alpha = \frac{\pi}{2}, \pm\frac{\pi}{6})$	$C_{2\alpha}$
70	$C_{2\alpha}, S_z^{2\alpha}(\alpha \neq \frac{\pi}{2}, \pm\frac{\pi}{6};\ \tau_o \notin \{G, A, B, C\}$ when $\alpha = 0, \pm\frac{\pi}{3})$	$C_{2\alpha}$
71	$C_{2\alpha}, C_z^{2(\alpha-\frac{\pi}{2})}, m_{(\alpha+\frac{\pi}{6})}, S_z^{2\alpha}(\alpha \neq \frac{\pi}{2}, \pm\frac{\pi}{6};\ \tau_o \notin \{G, A, B, C\}$ when $\alpha = 0, \pm\frac{\pi}{3})$	$C_{2\alpha}$
72	$C_{2\alpha}, S_z^{2(\alpha-\frac{\pi}{2})}, m_{(\alpha+\frac{\pi}{6})}, C_z^{2\alpha}(\alpha \neq 0, \pm\frac{\pi}{3};\ \tau_o \notin \{G, A, B, C\}$ when $\alpha = \frac{\pi}{2}, \pm\frac{\pi}{6})$	$C_{2\alpha}$
73	$C_{2\alpha}$	$C_{2\alpha}$
	$S_{4z}^{+}, S_{4z}^{-}, S_z^{\frac{\pi}{6}}, S_z^{\frac{5\pi}{6}}, S_z^{-\frac{\pi}{6}}, S_z^{-\frac{5\pi}{6}}$	S_{4z}
75	$C_{2\alpha}, m_{\alpha}$	$C_{2\alpha}$
	$S_{4z}^{+}, S_{4z}^{-}, S_z^{\frac{\pi}{6}}, S_z^{\frac{5\pi}{6}}, S_z^{-\frac{\pi}{6}}, S_z^{-\frac{5\pi}{6}}, C_{4z}^{+}, C_{4z}^{-}, C_z^{\frac{\pi}{6}}, C_z^{\frac{5\pi}{6}}, C_z^{-\frac{\pi}{6}}, C_z^{-\frac{5\pi}{6}}$	S_{4z}
76	$C_{2\alpha}, C_z^{2\alpha}$	$C_{2\alpha}$
	$S_{4z}^{+}, S_{4z}^{-}, S_z^{\frac{\pi}{6}}, S_z^{\frac{5\pi}{6}}, S_z^{-\frac{\pi}{6}}, S_z^{-\frac{5\pi}{6}}, m_{\frac{\pi}{12}}, m_{\frac{\pi}{4}}, m_{\frac{5\pi}{12}}, m_{\frac{7\pi}{12}}, m_{\frac{3\pi}{4}}, m_{\frac{11\pi}{12}}$	S_{4z}
77	$C_{2\alpha}, S_z^{2\alpha}(\alpha \neq 0, \frac{\pi}{2}, \pm\frac{\pi}{3}, \pm\frac{\pi}{6})$	$C_{2\alpha}$
	$S_{4z}^{+}, S_{4z}^{-}, S_z^{\frac{\pi}{6}}, S_z^{\frac{5\pi}{6}}, S_z^{-\frac{\pi}{6}}, S_z^{-\frac{5\pi}{6}}, C_2^{\frac{\pi}{12}}, C_2^{\frac{\pi}{4}}, C_2^{\frac{5\pi}{12}}, C_2^{\frac{7\pi}{12}}, C_2^{\frac{3\pi}{4}}, C_2^{\frac{11\pi}{12}}$	S_{4z}
78	$C_{2\alpha}, m_{\alpha}, S_z^{2(\alpha-\frac{\pi}{2})}, C_z^{2(\alpha-\frac{\pi}{2})}(\alpha \neq 0, \pm\frac{\pi}{3};\ \tau_o \notin \{G, A, B, C\}$ when $\alpha = \frac{\pi}{2}, \pm\frac{\pi}{6}))$	$C_{2\alpha}$
79	$C_{2\alpha}, m_{\alpha}, S_z^{2\alpha}, C_z^{2\alpha}(\alpha \neq \frac{\pi}{2}, \pm\frac{\pi}{6};\ \tau_o \notin \{G, A, B, C\}$ when $\alpha = 0, \pm\frac{\pi}{3})$	$C_{2\alpha}$
80	$C_{2\alpha}, m_{\alpha}, S_z^{2\alpha}, C_z^{2\alpha}(\alpha \neq 0, \frac{\pi}{2}, \pm\frac{\pi}{6}, \pm\frac{\pi}{3})$	$C_{2\alpha}$
	$C_{2\alpha}, m_{\alpha}, S_z^{2\alpha}, C_z^{2\alpha}(\alpha = \frac{n\pi}{12}, n = 1, 3, 5, 7, 9, 11)$	S_{4z}

TABLE II. Classification of bilayer stacking *A*-type altermagnets. Here we only consider the case where the translation part of stacking operation is G, i.e., the sliding operation, is not to be considered. We regard sliding operation as a constraint. For cases where the translation part of stacking operation is not G, the spin layer group of the bilayer can be determined by analyzing which symmetry is broken by the sliding operation compared to the case without sliding. For example, for the bilayer with ${}^{2}4/{}^{1}m$, if the translation part of stacking operation does not satisfy Eq. (12), S_{4z} will be broken, so the bilayer is not an altermagnet. Layer groups listed in the third and fourth columns represent the layer groups of the monolayers to form the bilayers, which correspond to the first column of Table I. The third column lists the case where the layers in bilayer can only be connected by $C_{2\alpha}$ and the fourth column lists the case where the layers in bilayer can be connected by S_{4z}, which corresponds to the third column of Table I. Therefore, each layer group corresponds to a case in Table I. The first column and the second column, respectively, list the characteristics of spin-momentum locking and nontrivial spin layer groups of BSAAs. When using this table, more attention should be paid to [34].

Spin-momentum locking	Nontrivial spin layer group	Layer group	
		$C_{2\alpha}$	S_{4z}
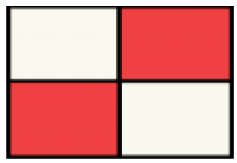	${}^{2}2/{}^{2}m_x$	1-2, 4-5, 8−18, 27−36	–
d wave	${}^{2}m{}^{2}m{}^{1}m$	3,6-7,19–26,37–48,50,57–60 ($\alpha \neq \pm\frac{\pi}{4}$ for 23–26, 37–48, and 59-60, $\alpha \neq 0, \frac{\pi}{2}$ for 57-58)	–
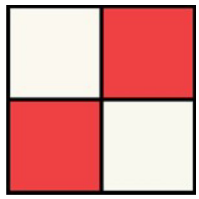	${}^{2}4/{}^{1}m$	–	3, 6-7, 19−22, 50, 73, 75-76
	${}^{2}4/{}^{1}m{}^{2}m{}^{1}m$	–	23−26, 37−48, 57−60, 77, 80
g wave 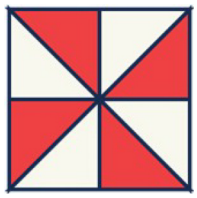	${}^{1}4/{}^{1}m{}^{2}m{}^{2}m$	49,51–56,61–64	–
i wave 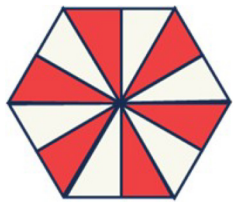	${}^{1}\bar{3}{}^{2}m$	65−72, 74, 78-79	–
	${}^{1}6/{}^{1}m{}^{2}m{}^{2}m$	73,75–77,80 ($\alpha \neq \frac{n\pi}{12}$, n=1,3,5,7,9,11 for 77, 80)	–

operation along the z direction and cannot affect the symmetry of the bilayer B whose layer group is $G_B = \{\hat{R}_B\}$. $\hat{O}$ is the nontrivial part of stacking operation, and $\hat{O} = \{\tau_o|O\}$, where τ_o represents the translation part and O is the point-group part. As a result, we can obtain the stacking model:

$$\begin{aligned} S &= \hat{R}_s S, \quad \forall\, \hat{R}_s \in G_s \\ B &= \hat{R}_B B, \quad \forall\, \hat{R}_B \in G_B \\ B &= S + S', \\ S' &= \hat{\tau}_z \hat{O} S. \end{aligned} \tag{1}$$

Due to considering only real-space transformations, this model is analogous to that of the bilayer stacking ferroelectricity (BSF) [33]. Therefore, we directly use the derivation results of BSF.

We only list the results about R^-, and more details are available in [33]. To ensure that the bilayer formed by stacking possesses the symmetry R^- ($R^- = \overline{E}$, m_z, or $C_{2\alpha}$), the stacking operations must satisfy the following equations:

if $R^- \in G_{s0}$,

$$O \in G_{s0}, \tag{2}$$

$$(E + R^-)\tau = \tau_{s0}, \tag{3}$$

$$\tau_o = \tau + \tau_s, \tag{4}$$

if $R^- \notin G_{s0}$,

$$O \in R^- G_{s0}, \tag{5}$$

$$(E + R^-)\tau = \tau_{s0}, \tag{6}$$

$$\tau_o = \tau + R^- \tau_s. \tag{7}$$

Equations (2) and (5) impose a constraint on the point-group part of stacking operation, while others impose a constraint on the translation part of stacking operation. G_{s0} contains all point-group symmetries of G_s. τ_s represents translation part of $\hat{R}_s$. τ_{s0} is an integer translation of the lattice vectors of the conventional cell of layer S. Moreover, to ensure that the bilayer possesses the symmetry S_{nz}, the stacking operations must satisfy the following equations:

if $S_{nz} \in G_{s0}$,

$$O \in G_{s0}, \tag{8}$$

$$(E + S_{nz})\tau = \tau_{s0}, \tag{9}$$

$$\tau_o = \tau + \tau_s, \tag{10}$$

if $S_{nz} \notin G_{s0}$,

$$C_{nz}^2 \in G_{s0}, \tag{11}$$

$$O \in S_{nz} G_{s0}, \tag{12}$$

$$(E+S_{nz})\tau = \tau_s^+ + \tau_{s0}, \tag{13}$$

$$\tau_o = \tau + R^- \tau_s. \tag{14}$$

Equation (11) imposes a constraint on G_{s0}. τ_s^+ is the translation part of $\hat{C}_{nz}^2$ in group G_s. The detailed derivation from Eq. (1) to Eqs. (2)–(14) is available in [33]. However, the general solution of these equations for each layer group is not available in [33].

We now derive all stacking operations to generate BSAA for each layer group, based on these equations. First, we notice that there must be $C_{nz}^2 \in G_{s0}$ when $S_{nz} \in G_{s0}$, and τ_s^+ is zero for any C_{nz}^2. Therefore, Eqs. (2)–(14) can be unified into the following equations:

For R^- ($R^- = \overline{E}, m_z, S_{nz}, C_{2\alpha}$),

$$(E+R^-)\tau = \tau_{s0}, \tag{15}$$

if $R^- \in G_{s0}$,

$$O \in G_{s0}, \tag{16}$$

$$\tau_o = \tau + \tau_s, \tag{17}$$

if $R^- \notin G_{s0}$,

$$O \in R^- G_{s0}, \tag{18}$$

$$\tau_o = \tau + R^- \tau_s. \tag{19}$$

Additionally, for S_{nz},

$$C_{nz}^2 \in G_{s0}. \tag{20}$$

Equation (20) determines whether it is possible for a specific monolayer to form the bilayer possessing S_{nz} symmetry through stacking. In summary, to ensure that the bilayer possesses the symmetry S_{nz}, the point-group part of space-group symmetry of layer S must contain C_{nz}^2 and the stacking operations must satisfy Eqs. (15)–(19). For other symmetries, the requirement is that the stacking operations must satisfy Eqs. (15)–(19). The 80 layer groups can be processed into 36 point groups G_{s0}. By applying the 36 point groups and the four possible R^- symmetries into Eq. (16) and (18), the point-group part of all stacking operations can be obtained for all layer groups.

We now focus on the translation part of the stacking operation, i.e., the solutions of Eq. (15). Because $E + \overline{E}$ is zero, there is no constraint on τ_o for $\overline{E}$, which implies that any sliding operation cannot break the inversion symmetry in the bilayer. For m_z, the solutions are $\tau_o = \{G, A, B, C\}$, where $G = (0, 0)$, $A = (\frac{1}{2}, 0)$, $B = (0, \frac{1}{2})$, $C = (\frac{1}{2}, \frac{1}{2})$, employing lattice vectors as basis vectors. $\tau_o = G$ means no translation. If the system is a centered rectangular lattice, $\tau_o = \{G, A, B, C, G', A', B', C'\}$ for m_z, where $G' = (\frac{1}{4}, \frac{1}{4})$, $A' = (\frac{3}{4}, \frac{1}{4})$, $B' = (\frac{1}{4}, \frac{3}{4})$, $G' = (\frac{3}{4}, \frac{3}{4})$. For $C_{2\alpha}$, translation of arbitrary length perpendicular to the vector $[\cos(\alpha), \sin(\alpha), 0]$, as well as translations by half of the lattice vector in the direction of vector $[\cos(\alpha), \sin(\alpha), 0]$, and their combinations, are all permitted. For S_{3z}, τ_o is only equal to G, which implies that any sliding operation can break it. For S_{6z}, $\tau_o = \{G, M, N\}$ are obtained, where $M = (\frac{1}{3}, \frac{2}{3}), N = (\frac{2}{3}, \frac{1}{3})$. For S_{4z}, the solutions of τ_o will not affect the results of this paper, and different lattices have different solutions. Therefore, we provide only a general solution

$$\begin{aligned} \tau_x &= \tfrac{1}{2}(\tau_{s0x} + \tau_{s0y}), \\ \tau_y &= \tfrac{1}{2}(\tau_{s0y} - \tau_{s0x}), \end{aligned} \tag{21}$$

where τ_x and τ_y are the x component and y component of τ, respectively. One of the lattice vectors of the conventional cell is chosen to serve as the x axis.

By excluding the stacking operations that generate $\{\overline{E}, m_z\}$ in the bilayer from those that generate $\{C_{2\alpha}, S_{nz}\}$ in the bilayer for each layer group, all BSAAs are obtained, as listed in Table I. The second column of Table I lists all stacking operations to form BSAA, for a ferromagnetic monolayer with layer group listed in the first column. The third column lists the symmetry exchanging the positions of two ferromagnetic layers in the bilayer under the stacking operation listed in the second column.

Based on Table I, we derive the following three conclusions. First, only 17 layer groups can realize intrinsic *A*-type altermagnetism, including layer group numbers 8–10, 19–22, 50, 53-54, 57–60, 67-68, 76. We regard the bilayer as intrinsic *A*-type altermagnet, if the top layer is obtained by translating the bottom layer along the z direction without any other operations and it possesses *A*-type altermagnetism. Because the stacking operation is $\hat{\tau}_z\{0|E\}$, the symmetry of monolayer is the same as bilayer, i.e., they possess the same layer group. Therefore, this conclusion has two implications. The first one is that only ferromagnetic monolayers with these layer groups can form BSAA through $\hat{\tau}_z\{0|E\}$, without any other operations. The second is that all 2D *A*-type altermagnets must belong to these 17 layer groups. Obviously, not all 2D *A*-type altermagnets can be regarded as being formed by two sublattices through stacking operation $\hat{\tau}_z\{0|E\}$. This is because the minimum energy structure of 2D materials

may require sliding, twisting, or other adjustments to achieve. However, it will not affect our result. If the minimum energy structure possesses 2D *A*-type altermagnetism, its layer group must belong to these 17 layer groups. In other words, *A*-type antiferromagnetic bilayers that belong to these 17 layer groups will exhibit altermagnetism. Furthermore, the layer group of all BSAAs belong to these 17 layer groups.

Second, it is impossible to connect the two sublattices of BSAA using S_{3z} or S_{6z}. This is because the emergency of S_{6z} is always accompanied by inversion symmetry, and the emergency of S_{3z} is always accompanied by m_z symmetry. Moreover, the inversion symmetry in the bilayer cannot be broken by sliding operation, and any sliding operation will break S_{3z} symmetry. In fact, this result is consistent with our previous work [26]. All 2D altermagnets are described using seven spin layer groups. There are not spin-group symmetry $[C_2||S_{3z}]$ and $[C_2||S_{6z}]$ in all spin layer groups. It implies that it is impossible to connect the two sublattices of all 2D altermagnets using S_{3z} or S_{6z}. Therefore, this conclusion is also applicable to all 2D altermagnets.

Finally, $C_{2\alpha}$, where α is an arbitrary angle within the range from 0 to π, is a general stacking operation to generate BSAA for an arbitrary monolayer. Meanwhile, we notice that not all *A*-type antiferromagnetic bilayers can generate altermagnetism only through twisting. From a stacking perspective, the twisting can be regarded as stacking operation $C_z^{2\alpha}$. Based on Table I, it is not a general stacking operation to generate BSAA. In addition, we notice that a related work [31] proposed that a flipping operation $C_{2\alpha}$ combined with a twisting operation C_z^{β} is a general way to construct 2D altermagnets. In fact, the combined effect of these two operations is equivalent to a flipping operation. Consequently, our conclusion is consistent with theirs.

To further understand and utilize Table I, we use spin layer groups to classify the BSAAs listed in Table I, and also provide the corresponding spin-momentum locking, as shown in Table II. Here we only consider the case in which sliding operation is neglected. The sliding operation can be regarded as a constraint. If there exists any sliding operation in the practical applications, the translation part of stacking operations generating bilayers with symmetry $C_{2\alpha}$ or S_{4z} can be used to determine which symmetry is broken and then its spin layer group. The analysis of $NiZrI_6$ in Sec. V can serve as a reference. Once the spin layer group of the system is determined, the characteristics of spin-momentum locking can be obtained. Table I provides guidance on how to construct BSAA based on a ferromagnetic monolayer, while Table II details the characteristics of spin-momentum locking of the BSAAs constructed according to Table I. We recommend using both tables together. Table II greatly facilitates future research on BSAA, as it provides information on spin-momentum locking in the BSAA based on the layer group of the monolayer, eliminating the need for a detailed symmetry analysis.

III. BILAYER WITH INTRINSIC *A*-TYPE ALTERMAGNETISM

According to the first conclusion of the last section, a bilayer characterized by intralayer ferromagnetic coupling and interlayer antiferromagnetic coupling, and belonging to one of 17 layer groups, exhibits *A*-type altermagnetism. Based on these layer groups, we search for BSAA in van der Waals bilayer database (BiDB) [35] as the example of BSAA. First, we select out materials with these 17 layer groups. Then, we examine their magnetic coupling properties. If the magnetic configuration is *A* type, we stop our search. A comprehensive search of the database is not conducted.

Based on the above approach, we predict that bilayer $NiZrCl_6$, in which the top layer is obtained by applying τ_z on the bottom layer, exhibits intrinsic *A*-type altermagnetism. The crystal structure of bilayer $NiZrCl_6$ is schematically illustrated in Fig. 1(a), with red and blue colors representing the sublattices with opposite spins in *A*-type altermagnetism. This structure is stable, according to the data in BiDB. The monolayer $NiZrCl_6$ exhibits ferromagnetism, which has been reported previously [36]. Meanwhile, the layer group number of monolayer $NiZrCl_6$ is No. 67, which surely belongs to the 17 layer groups. Therefore, as long as the interlayer magnetic coupling is antiferromagnetic, the bilayer $NiZrCl_6$ is BSAA, according to our theory. Using the first-principles calculation, we compare the energies of different magnetic configurations, ferromagnetic and *A*-type altermagnetic. The energy of *A*-type altermagnetic state is 0.25 meV/f.u. lower than that of the ferromagnetic state, which indicates that its magnetic ground state is *A*-type altermagnetism.

Through symmetry analysis, the spin layer group of bilayer $NiZrCl_6$ is determined as ${}^1\bar{3}^2m$, which is consistent with Table II. The sublattices are related by three twofold rotation symmetries along the rotational axes within *xy* plane, as illustrated in Fig. 1(a), but not by inversion symmetry or mirror symmetry parallel to *xy* plane. This is why bilayer $NiZrCl_6$ exhibits altermagntism. Consequently, the spin-momentum locking of bilayer $NiZrCl_6$ is determined by the symmetries $[C_2||\{C_2^{1\bar{1}0}, C_2^{120}, C_2^{210}\}]$, as illustrated in Fig. 1(b). The **k** paths, related by $C_2^{1\bar{1}0}$ (C_2^{120}, C_2^{210}) but not separated by a reciprocal lattice vector, have opposite spin signs. Figure 1(c) shows the DFT calculated band structure without SOC and the employed **k** path is shown in Fig. 1(b). The spin-splitting band structure along K1-Γ-K2 and the zero net magnetic moment implies that bilayer $NiZrCl_6$ is an altermagnet. This result is consistent with our theory. The bilayer $NiZrCl_6$ corresponds to the case where layer group is No. 67 and $\alpha = \frac{\pi}{2}$ in Table I.

IV. TWISTED-BILAYER WITH *A*-TYPE ALTERMAGNETISM

Twisted-bilayer systems with *A*-type altermagnetism have been researched [30,31]. It is noteworthy that a twisted bilayer can be regarded as two single layers in which the top layer is rotated and then stacked onto the bottom layer. In this paper, it corresponds to the stacking operation $C_z^{2\alpha}$. In this case, 2α is the twisting angle. Therefore, we posit that the twisted-bilayer with *A*-type altermagnetism is also BSAA. We here take twisted-bilayer $NiCl_2$ and CrOCl as examples of BSAA to verify our results.

The twisted-bilayer $NiCl_2$ has been predicted as an *A*-type altermagnet in a previous paper [30]. The layer group number of the monolayer 1T phase $NiCl_2$ is No. 72. Based

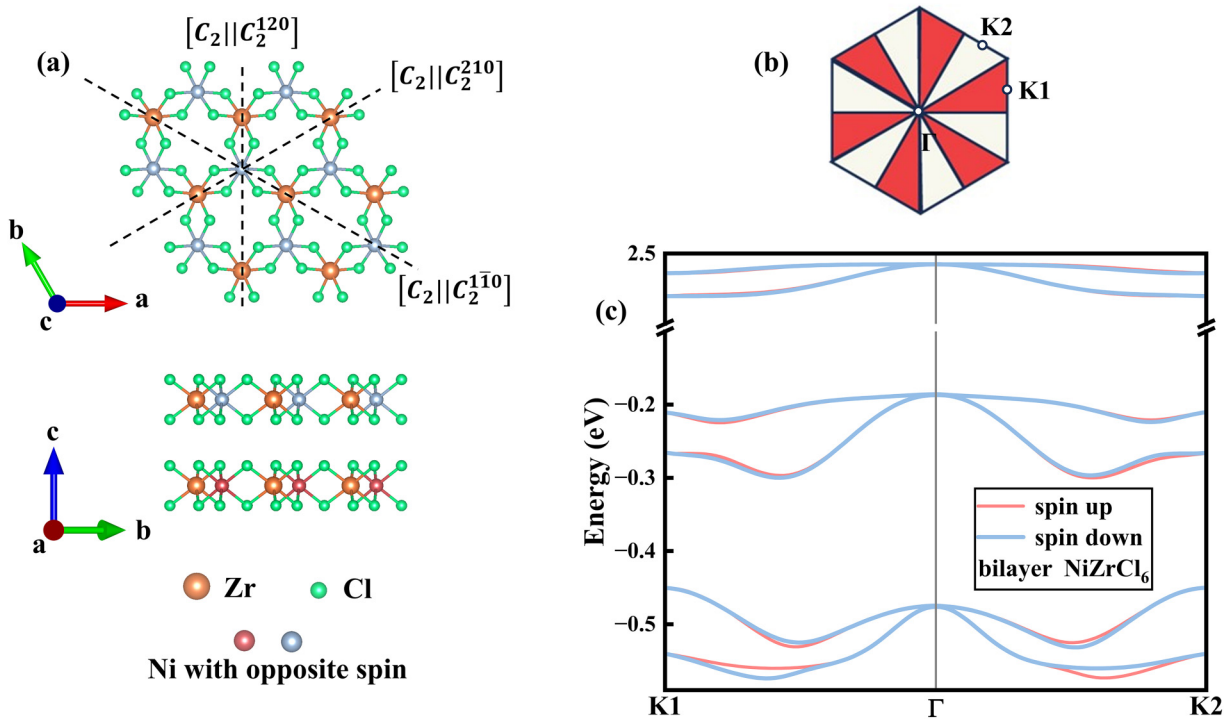

FIG. 1. The crystal structure and nonrelativistic band structure of bilayer $NiZrCl_6$. (a) The crystal structure of bilayer $NiZrCl_6$, where red and blue colors represent the opposite spin sublattices. Three spin-group symmetries, which interconnect two ferromagnetic layers, have been shown in (a). (b) The Brillouin zone of bilayer $NiZrCl_6$, in which the different colors represent opposite spins, and high-symmetry points used to calculate band structure. (c) The band structure of bilayer $NiZrCl_6$ without SOC along **k** path K1-Γ-K2 is spin splitting, where red and blue lines represent the opposite spin channels. The spin-splitting band structure in (c) illustrates that bilayer $NiZrCl_6$ exhibits altermagnetism.

on Table I, to achieve *A*-type altermagnetism, $\alpha = \{0, \pm\frac{\pi}{3}\}$ are forbidden, but the moiré angle of the structure, including 13.17°, 21.79°, 27.79°, 32.21°, 38.21°, and 46.83°, are permitted. This is because the inversion symmetry is broken by twisting with a moiré angle, but preserved by twisting with $2\alpha = \{0, \pm\frac{2\pi}{3}\}$. This result is consistent with the previous research [30]. It is noteworthy that when twisting angle is equal to π or $\pm\frac{\pi}{3}$, the mirror symmetry through the xy plane, m_z, is generated in the twisted-bilayer $NiCl_2$. Therefore, to achieve *A*-type altermagnetism, the extra sliding is necessary for twisted-bilayer $NiCl_2$ with a twisting angle of π or $\pm\frac{\pi}{3}$, as listed in Table I.

We now focus on the twisted-bilayer $NiCl_2$ with a twisting angle of 21.79°. The crystal structure is schematically illustrated in Fig. 2(a). Through symmetry analysis, we determine that its spin layer group is ${}^1\bar{3}^2m$ and its layer group number is 67. As mentioned earlier, for the material with 2D *A*-type altermagnetism, it must be one of the 17 layer groups. Interestingly, the twisted-bilayer $NiCl_2$ has the same spin layer group with $NiZrCl_6$, which has been discussed in Sec. III. Consequently, they have the same spin-momentum locking. We use the same **k** path, as illusctrated in Fig. 2(c), to calculate band structure. Figure 2(b) shows the DFT calculated band structure without SOC, which demonstrates that it clearly exhibits *A*-type altermagnetism.

The monolayer CrOCl has been studied in the previous work [37]. It was suggested that monolayer CrOCl can be easily fabricated from its bulk counterpart, and it is a 2D intrinsic ferromagnet. Meanwhile, its bulk counterpart exhibits antiferromagnetism. However, the twisted-bilayer CrOCl was never studied previously. Subsequently, we demonstrate that twisted-bilayer CrOCl with twisting angle of 90° exhibits *A*-type altermagnetism.

From a symmetry perspective, the layer group of the monolayer CrOCl is No. 46. According to Table I, under the stacking operation $\{G|C_z^{\frac{\pi}{2}}\}$, two monolayers of CrOCl can form a BSAA, if their interlayer coupling is antiferromagnetic. The stacking operation $\{G|C_z^{\frac{\pi}{2}}\}$ is equivalent to twisting operation with twisting angle of 90°. The crystal structure of twisted-bilayer CrOCl is schematically illustrated in Fig. 3(a), with red and blue colors representing the sublattices with opposite spins in *A*-type altermagnetism. Two side views indicate that it exhibits a S_{4z} symmetry. Through DFT calculation, it is suggested that the energy of *A*-type altermagnetic state, as illustrated in Fig. 3(a), is 0.23 meV/f.u. lower than that of the ferromagnetic state, which implies that the magnetic ground state of the twisted-bilayer CrOCl is *A*-type altermagnetism, i.e., its interlayer coupling is antiferromagnetic. Consequently, according to our results on BSAA, the twisted-bilayer CrOCl with twisting angle of 90° exhibits *A*-type altermagnetism. Furthermore, according to Table II, its spin layer group is ${}^24/{}^1m^2{}^1m$, and its characteristic of spin-momentum locking is illustrated in Fig. 3(b).

In order to confirm the analysis above, we calculated its band structure without SOC using the first-principles calculation, and the employed **k** path is shown in Fig. 3(b). The calculated band structure, which is shown in Fig. 3(c), implies

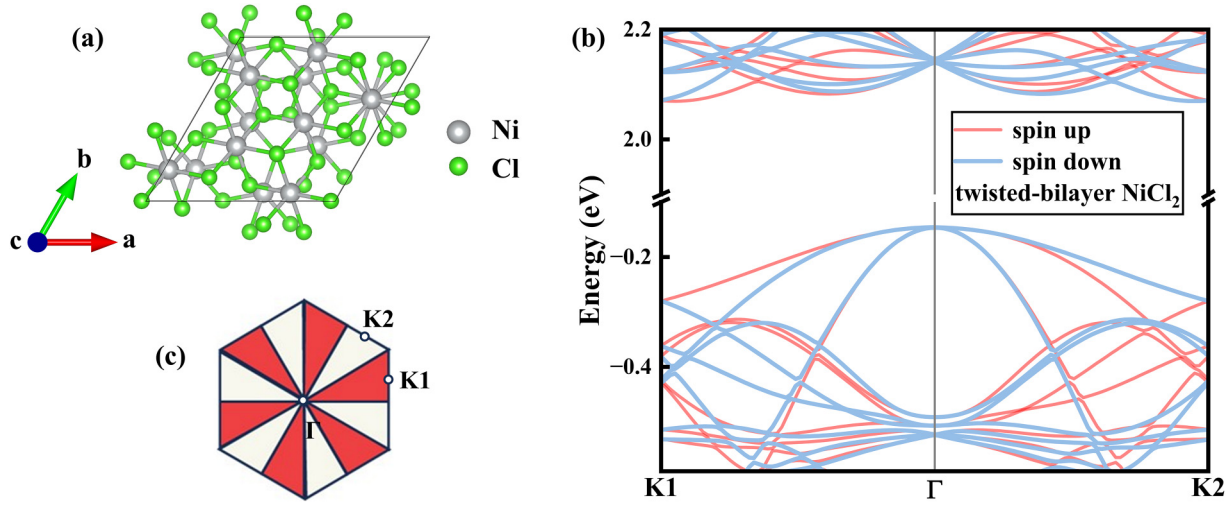

FIG. 2. The crystal structure and nonrelativistic band structure of twisted-bilayer $NiCl_2$ with a twisting angle of 21.79°. (a) The crystal structure of twisted-bilayer $NiCl_2$. (b) The band structure of twisted-bilayer $NiCl_2$ without SOC along **k** path K1-Γ-K2 is spin splitting, where red and blue lines represent the opposite spin channels. (c) The Brillouin zone of twisted-bilayer $NiCl_2$, in which the different colors represent opposite spins, and high-symmetry points used to calculate band structure. The spin-splitting band structure in (b) illustrates that twisted-bilayer $NiCl_2$ exhibits altermagnetism.

that the twisted-bilayer CrOCl is an altermagnet, which is consistent with the above discussion. Our results have once again been confirmed. Due to its large spin-splitting band structure, ease of exfoliation and stability, we believe that the twisted-bilayer CrOCl is well suited for experimental validation of BSAA.

V. REPORTED MATERIALS OF BSAA

Recently, research on bilayers with altermagnetism has gained significant attention [29–32]. Some reported materials belong to the class of BSAA, while others do not. Here we identify some reported materials as BSAAs and list them in

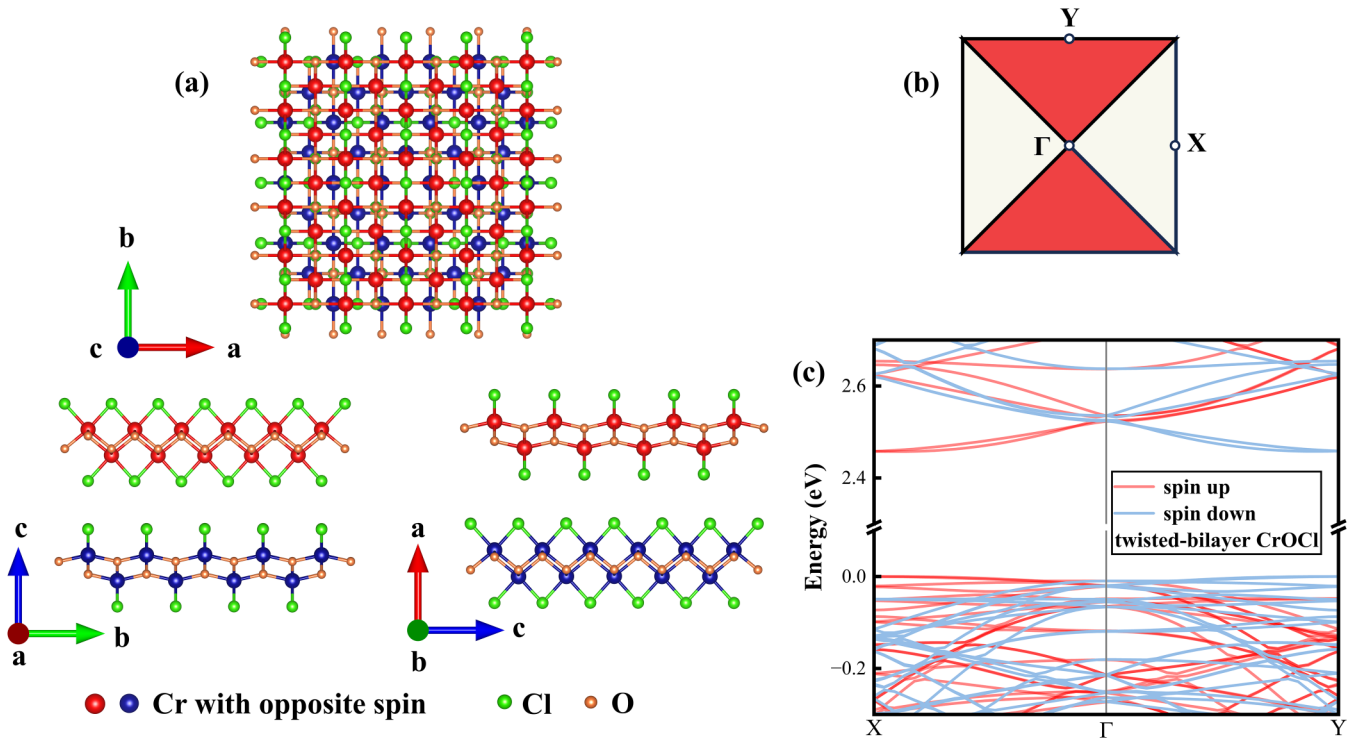

FIG. 3. The crystal structure and nonrelativistic band structure of twisted-bilayer CrOCl with a twisting angle of 90°. (a) The crystal structure of twisted-bilayer CrOCl. (b) The Brillouin zone of twisted-bilayer CrOCl, in which the different colors represent opposite spins, and high-symmetry points used to calculate band structure. (c) The band structure of twisted-bilayer CrOCl without SOC along **k** path $X-\Gamma-Y$ is spin splitting, where red and blue lines represent the opposite spin channels. The spin-splitting band structure in (c) illustrates that twisted-bilayer CrOCl exhibits altermagnetism.

TABLE III. A summary of reported BSAAs. Here we list some examples of the BSAA which have been reported in previous works. The materials listed in the first column possess layer group listed in the second column. Using the stacking operations listed in the fourth column, these materials have been constructed into the bilayers with *A*-type altermagnetism in previous works. Based on Table I and their layer groups, the stacking operations generating BSAAs can be obtained and listed in the third column. Through comparing the third and fourth columns, it can be found that our results are consistent with these previous works.

Material	Layer group	Point-group part of stacking operation	Stacking operation in the reported BSAAs
$NiCl_2$	72	$C_{2\alpha}, S_z^{2(\alpha-\frac{\pi}{2})}, m_{(\alpha+\frac{\pi}{6})}, C_z^{2\alpha}$ $(\alpha \neq 0, \pm\frac{\pi}{3};\ \tau_o \notin \{G, A, B, C\}$ when $\alpha = \frac{\pi}{2}, \pm\frac{\pi}{6})$	$\{G\|C_z^\beta\}$ [30] ($\beta =$ 13.17°, 21.79°, 27.79°, 32.21°, 38.21° and 46.83°)
CrI_3	71	$C_{2\alpha}, C_z^{2(\alpha-\frac{\pi}{2})}, m_{(\alpha+\frac{\pi}{6})}, S_z^{2\alpha}$ $(\alpha \neq \frac{\pi}{2}, \pm\frac{\pi}{6};\ \tau_o \notin \{G, A, B, C\}$ when $\alpha = 0, \pm\frac{\pi}{3})$	$\{G\|C_z^\beta\}(\beta = 21.79°)$[30] and $\{G\|C_{2\alpha}\}$ [31]
CrSBr	46	$C_{2\alpha}, C_z^{2\alpha}, m_\alpha, S_z^{2\alpha}(\alpha \neq 0, \frac{\pi}{2})$	$\{G\|C_z^{\frac{\pi}{2}}\}$ [30]
VOBr	46	$C_{2\alpha}, C_z^{2\alpha}, m_\alpha, S_z^{2\alpha}(\alpha \neq 0, \frac{\pi}{2})$	$\{G\|C_{2\alpha}\}$ [31]
Co_2S_2	64	$C_{2\alpha}, S_z^{2\alpha}, C_z^{2\alpha}, m_\alpha(\alpha \neq 0, \pm\frac{\pi}{4}, \frac{\pi}{2})$	$\{G\|C_{2\alpha}\}$ [31]
$MnBi_2Te_4$	72	$C_{2\alpha}, S_z^{2(\alpha-\frac{\pi}{2})}, m_{(\alpha+\frac{\pi}{6})}, C_z^{2\alpha}$ $(\alpha \neq 0, \pm\frac{\pi}{3};\ \tau_o \notin \{G, A, B, C\}$ when $\alpha = \frac{\pi}{2}, \pm\frac{\pi}{6})$	$\{G\|C_{2\alpha}\}$ [31]
$NiZrI_6$	67	$C_{2\alpha}, C_z^{2(\alpha-\frac{\pi}{2})}$	$\{G\|E\}$ $\{A\|E\}$ $\{C\|E\}$ [32]
CrBrSe	46	$C_{2\alpha}, C_z^{2\alpha}, m_\alpha, S_z^{2\alpha}(\alpha \neq 0, \frac{\pi}{2})$	$\{G\|C_z^\beta\}(\beta = 109.46°)$ [32]

Table III. Subsequently, we offer a concise discussion of these materials and analyze the emergence of altermagnetism from the perspective of this work.

As is known to all, the 2D material CrI_3 exhibits intralayer ferromagnetic and interlayer antiferromagnetic coupling, i.e., *A*-type antiferromagnetism. As its layer group is No. 71, which does not belong to 17 layer groups mentioned above, bilayer CrI_3 is a conventional antiferromagnet under normal stacking. From a symmetry perspective, monolayer CrI_3 exhibits inversion symmetry and it cannot be broken by any sliding operation. Therefore, bilayer CrI_3 constructed by stacking operation $\{\tau_o|E\}$ also exhibits inversion symmetry, which will protect spin-degeneracy band in the whole Brillouin zone. However, a twisting [30] or flipping [31] operation will break this symmetry, leading to the emergence of altermagnetism. This is why the previous works can construct bilayer CrI_3 with *A*-type altermagnetism. These results are consistent with Table I. Moreover, according to Table II, these bilayers both possess the spin layer group ${}^1\overline{3}^2m$ and *i*-wave altermagnetism.

We then focus on CrSBr [30], VOBr [31], and CrBrSe [32]. These materials have been studied in different works and constructed into BSAAs using different stacking operations. However, it is noteworthy that they all belong to layer group No. 46, so they can be constructed into BSAAs through the same stacking operations from the perspective of this work. As the layer group No. 46 does not belong to the 17 layer groups mentioned above, their bilayers are all conventional *A*-type antiferromagnets under normal stacking, which also verifies conclusion (i) in our work. Through symmetry analysis, it can be observed that they all exhibit inversion symmetry and mirror symmetry parallel to the *xy* plane. According to Table I, a twisting or flipping operation will simultaneously break these symmetries, which is consistent with the previous works. Moreover, according to Table II, the bilayer CrSBr with twisting angle of 90° belongs to the spin layer group ${}^24/{}^1m^2m^1m$, while bilayer CrBrSe with twisting angle of 109.46° and VOBr with stacking operation $\{G|C_{2\alpha}\}$ belong to ${}^2m^2m^1m$. But, they all exhibit *d*-wave altermagnetism. In summary, our discussion and results in this paper are universally applicable. The above discussion implies that these materials all are BSAAs. All of them can be used to support our results.

VI. CONCLUSION AND DISCUSSION

In summary, we propose a concept of bilayer stacking *A*-type altermagnet (BSAA), deduce all BSAAs for all layer groups, and provide two distinct examples of BSAAs. Our research has significantly broadened the range of candidate materials for 2D altermagnets. Based on all BSAAs we have derived, we obtain three intriguing findings: (i) Only 17 layer groups can realize intrinsic *A*-type altermagnetism. All 2D *A*-type altermagnets must belong to these 17 layer groups, which has never been reported previously. Of course, all BSAAs listed in Table I belong to these 17 layer groups. *A*-type antiferromagnetic bilayers that belong to these 17 layer groups will exhibit altermagnetism. (ii) It is impossible to connect the two sublattices of BSAA using S_{3z} or S_{6z}. Combining the past research [26], we find that this conclusion is applicable to all 2D altermagnets. (iii) $C_{2\alpha}$ is a general stacking operation to generate BSAA for an arbitrary monolayer.

Based on symmetry analysis and DFT calculation, we predict a 2D altermagnet, the bilayer $NiZrCl_6$, which has never been reported in the past. Meanwhile, we notice that the previously reported twisted-bilayer *A*-type altermagnets are contained within the class of BSAA. We use twisted-bilayer $NiCl_2$ and CrOCl as examples of BSAA. Finally, we identify some materials as BSAA and provide a brief discussion.

It is noteworthy that the concept of van der Waals materials is not mentioned in the above discussion. In fact, according to the requirements for generating two-dimensional altermagnetism, whether a two-dimensional system exhibits altermagnetism depends solely on its symmetry and magnetic order. The fact that it is a van der Waals material or not does not affect the emergence of altermagnetism. If monolayers with and without van der Waals structures share the same symmetry, they can be assembled into bilayers with altermagnetism using the same stacking operations. Therefore, we believe that our results are applicable not only to van der Waals materials, but also to non-van der Waals materials, which implies that our results have general applicability.

Note added. Recently, we noticed a paper which explores a material similar to the one used in our work [32]. They studied the material $NiZrI_6$, which has a structure analogous to that of the material $NiZrCl_6$. Its layer group is No. 67, which belongs to the 17 layer groups. Therefore, bilayer $NiZrI_6$ with stacking operation $\{G|E\}$ also exhibits intrinsic A-type altermagnetism. According to Table II, its spin layer group is ${}^{1}\bar{3}^{2}m$, which means that it exhibits i-wave altermagnetism. In addition, the bilayers of $NiZrI_6$ with stacking operations $\{A|E\}$ and $\{C|E\}$ were studied, and it is suggested that they all exhibit altermagnetism. From the perspective of our work, this is because the symmetry $C_{2\alpha}$ is not broken by these two sliding operations. According to the discussion regarding the translation part of stacking operation in Sec. II, translations by half of the lattice vector in the direction of vector $[\cos(\alpha), \sin(\alpha), 0]$ will preserve the symmetry $C_{2\alpha}$ in the bilayer. Similar to $NiZrCl_6$, monolayer $NiZrI_6$ also exhibits three $C_{2\alpha}$ symmetries. However, the three rotational axes are oriented at 60° angles to each other. Therefore, the stacking operations $\{A|E\}$ and $\{C|E\}$ solely preserve one $C_{2\alpha}$ symmetry, respectively. Consequently, their spin layer groups are ${}^{2}2/{}^{2}m_x$. It is noteworthy that the sliding operations A and C transform bilayer $NiZrI_6$ from i-wave altermagnetism to d-wave altermagnetism.

ACKNOWLEDGMENTS

This work is financially supported by National Natural Science Foundation of China (Grant No. 12074126). This work is partially supported by High Performance Computing Platform of South China University of Technology.

TABLE IV. The parameters for calculation. The lattice vectors of $NiCl_2$ and CrOCl listed in the third column, a/b, are the lattice vectors of the superlattice of bilayer $NiCl_2$ and CrOCl. The interlayer distance represents the distance between two layers in bilayer.

Material	Hubbard U (eV)	a/b (Å)	k mesh	Interlayer distance (Å)
$NiZrCl_6$	3 [36]	6.20	14×14 × 1	3.18
$NiCl_2$	3	9.14	6×6×1	3.33
CrOCl	7 [37]	15.86	2×2 × 1	3.30

APPENDIX: COMPUTATIONAL DETAILS

All DFT calculations were performed using the Vienna *ab initio* simulation package (VASP) [38,39], employing the projector-augmented wave (PAW) method [40] based on density functional theory. For the exchange-correlation functional, we use the generalized gradient approximation (GGA) with Perdew-Burke-Ernzerhof (PBE) functional [41], along with Hubbard U correction [42]. The parameters for calculation are listed in Table IV. A cutoff energy of 600 eV was set for the plane-wave basis. The structure was relaxed until the forces on atoms were below 0.01 eV/Å and the convergence criteria were 1×10^{-7} eV for the energy difference in electronic self-consistent calculation. A vacuum of 18 Å was constructed perpendicular to the material plane. We utilize the DFT-D3 approach [43] to correct van der Waals (vdW) interaction. The SOC effect was not considered in calculations.

Regarding CrOCl, we first performed a structural optimization for the monolayer, obtaining lattice constants of 3.966 and 3.270 Å, which are close to those reported in previous studies [37]. Next, we applied a uniaxial strain of 2.93% along the short axis and expanded the cell to 4×5 × 1. We then rotated one layer by 90°, and stacked it onto the other layer. Finally, we performed a structural optimization with the lattice vectors unchanged.

[1] I. Mazin, Altermagnetism then and now, Physics **17**, 4 (2024).
[2] L. Šmejkal, J. Sinova, and T. Jungwirth, Emerging research landscape of altermagnetism, Phys. Rev. X **12**, 040501 (2022).
[3] L. Bai, W. Feng, S. Liu, L. Šmejkal, Y. Mokrousov, and Y. Yao, Altermagnetism: Exploring new frontiers in magnetism and spintronics, Adv. Funct. Mater. **2024**, 2409327 (2024).
[4] I. Mazin, Editorial: Altermagnetism—a new punch line of fundamental magnetism, Phys. Rev. X **12**, 040002 (2022).
[5] I. I. Mazin, Altermagnetism in MnTe: Origin, predicted manifestations, and routes to detwinning, Phys. Rev. B **107**, L100418 (2023).
[6] T. A. Maier and S. Okamoto, Weak-coupling theory of neutron scattering as a probe of altermagnetism, Phys. Rev. B **108**, L100402 (2023).
[7] Z. Feng, X. Zhou, L. Šmejkal, L. Wu, Z. Zhu, H. Guo, R. González-Hernández, X. Wang, H. Yan, P. Qin *et al.*, An anomalous hall effect in altermagnetic ruthenium dioxide, Nat. Electron. **5**, 735 (2022).
[8] M. Naka, S. Hayami, H. Kusunose, Y. Yanagi, Y. Motome, and H. Seo, Spin current generation in organic antiferromagnets, Nat. Commun. **10**, 4305 (2019).
[9] A. Bose, N. J. Schreiber, R. Jain, D.-F. Shao, H. P. Nair, J. Sun, X. S. Zhang, D. A. Muller, E. Y. Tsymbal, D. G. Schlom *et al.*, Tilted spin current generated by the collinear antiferromagnet ruthenium dioxide, Nat. Electron. **5**, 267 (2022).
[10] K.-H. Ahn, A. Hariki, K.-W. Lee, and J. Kuneš, Antiferromagnetism in RuO_2 as d-wave pomeranchuk instability, Phys. Rev. B **99**, 184432 (2019).

[11] P. A. McClarty and J. G. Rau, Landau theory of altermagnetism, Phys. Rev. Lett. **132**, 176702 (2024).

[12] L. Šmejkal, R. González-Hernández, T. Jungwirth, and J. Sinova, Crystal time-reversal symmetry breaking and spontaneous Hall effect in collinear antiferromagnets, Sci. Adv. **6**, eaaz8809 (2020).

[13] S. Hayami, Y. Yanagi, and H. Kusunose, Momentum-dependent spin splitting by collinear antiferromagnetic ordering, J. Phys. Soc. Jpn. **88**, 123702 (2019).

[14] L.-D. Yuan, Z. Wang, J.-W. Luo, E. I. Rashba, and A. Zunger, Giant momentum-dependent spin splitting in centrosymmetric low-*Z* antiferromagnets, Phys. Rev. B **102**, 014422 (2020).

[15] I. I. Mazin, K. Koepernik, M. D. Johannes, R. González-Hernández, and L. Šmejkal, Prediction of unconventional magnetism in doped $FeSb_2$, Proc. Natl. Acad. Sci. USA **118**, e2108924118 (2021).

[16] H.-Y. Ma, M. Hu, N. Li, J. Liu, W. Yao, J.-F. Jia, and J. Liu, Multifunctional antiferromagnetic materials with giant piezomagnetism and noncollinear spin current, Nat. Commun. **12**, 2846 (2021).

[17] L. Šmejkal, J. Sinova, and T. Jungwirth, Beyond conventional ferromagnetism and antiferromagnetism: A phase with nonrelativistic spin and crystal rotation symmetry, Phys. Rev. X **12**, 031042 (2022).

[18] P. Liu, J. Li, J. Han, X. Wan, and Q. Liu, Spin-group symmetry in magnetic materials with negligible spin-orbit coupling, Phys. Rev. X **12**, 021016 (2022).

[19] S. Lee, S. Lee, S. Jung, J. Jung, D. Kim, Y. Lee, B. Seok, J. Kim, B. G. Park, L. Šmejkal, C.-J. Kang, and C. Kim, Broken kramers degeneracy in altermagnetic MnTe, Phys. Rev. Lett. **132**, 036702 (2024).

[20] S. Reimers, L. Odenbreit, L. Šmejkal, V. N. Strocov, P. Constantinou, A. B. Hellenes, R. Jaeschke Ubiergo, W. H. Campos, V. K. Bharadwaj, A. Chakraborty *et al.*, Direct observation of altermagnetic band splitting in CrSb thin films, Nat. Commun. **15**, 2116 (2024).

[21] L. Šmejkal, A. B. Hellenes, R. González-Hernández, J. Sinova, and T. Jungwirth, Giant and tunneling magnetoresistance in unconventional collinear antiferromagnets with nonrelativistic spin-momentum coupling, Phys. Rev. X **12**, 011028 (2022).

[22] R. González-Hernández, L. Šmejkal, K. Výborný, Y. Yahagi, J. Sinova, T. c. v. Jungwirth, and J. Železný, Efficient electrical spin splitter based on nonrelativistic collinear antiferromagnetism, Phys. Rev. Lett. **126**, 127701 (2021).

[23] S. Karube, T. Tanaka, D. Sugawara, N. Kadoguchi, M. Kohda, and J. Nitta, Observation of spin-splitter torque in collinear antiferromagnetic RuO_2, Phys. Rev. Lett. **129**, 137201 (2022).

[24] H. Bai, L. Han, X. Y. Feng, Y. J. Zhou, R. X. Su, Q. Wang, L. Y. Liao, W. X. Zhu, X. Z. Chen, F. Pan, X. L. Fan, and C. Song, Observation of spin splitting torque in a collinear antiferromagnet RuO_2, Phys. Rev. Lett. **128**, 197202 (2022).

[25] J. Sødequist and T. Olsen, Two-dimensional altermagnets from high throughput computational screening: Symmetry requirements, chiral magnons, and spin-orbit effects, Appl. Phys. Lett. **124**, 182409 (2024).

[26] S. Zeng and Y.-J. Zhao, Description of two-dimensional altermagnetism: Categorization using spin group theory, Phys. Rev. B **110**, 054406 (2024).

[27] I. Mazin, R. González-Hernández, and L. Šmejkal, Induced monolayer altermagnetism in $MnP(S,Se)_3$ and FeSe, arXiv:2309.02355.

[28] Q. Liu, J. Kang, P. Wang, W. Gao, Y. Qi, J. Zhao, and X. Jiang, Inverse magnetocaloric effect in altermagnetic 2d non-van der Waals FeX (X = S and Se) semiconductors, Adv. Funct. Mater. (2024).

[29] S. Sheoran and S. Bhattacharya, Nonrelativistic spin splittings and altermagnetism in twisted bilayers of centrosymmetric antiferromagnets, Phys. Rev. Mater. **8**, L051401 (2024).

[30] R. He, D. Wang, N. Luo, J. Zeng, K.-Q. Chen, and L.-M. Tang, Nonrelativistic spin-momentum coupling in antiferromagnetic twisted bilayers, Phys. Rev. Lett. **130**, 046401 (2023).

[31] Y. Liu, J. Yu, and C.-C. Liu, Twisted magnetic van der Waals bilayers: An ideal platform for altermagnetism, arXiv:2404.17146 [Phys. Rev. Lett. (to be published)].

[32] B. Pan, P. Zhou, P. Lyu, H. Xiao, X. Yang, and L. Sun, General stacking theory for altermagnetism in bilayer systems, Phys. Rev. Lett. **133**, 166701 (2024).

[33] J. Ji, G. Yu, C. Xu, and H. J. Xiang, General theory for bilayer stacking ferroelectricity, Phys. Rev. Lett. **130**, 146801 (2023).

[34] *Note*: Although we provide only the type of spin-momentum locking, the specific spin-momentum locking can be uniquely determined for certain spin layer groups. For ${}^{2}2/{}^{2}m_x$, ${}^{2}m^{2}m^{1}m$, ${}^{1}4/{}^{1}m^{2}m^{2}m$, ${}^{1}\bar{3}^{2}m$, and ${}^{1}6/{}^{1}m^{2}m^{2}m$, the real spin-momentum locking of the specific materials with these spin layer groups corresponds directly to the figures listed in the first column. For these materials, using these figures, one can determine whether a specific k path is spin degenerate or not. However, caution is needed when using the figure listed in the first column for ${}^{2}4/{}^{1}m$ and ${}^{2}4/{}^{1}m^{2}m^{1}m$. For ${}^{2}4/{}^{1}m$, its specific spin-momentum locking cannot be uniquely determined, as it does not contain a mirror symmetry perpendicular to the xy plane. However, it exhibits d-wave characteristics and fourfold symmetry, so the second figure in the first column is used to describe it. There are two cases for ${}^{2}4/{}^{1}m^{2}m^{1}m$: one is the second figure, and the other is Fig. 3(b). When analyzing a material with this group, the mirror symmetry perpendicular to the xy plane should be carefully identified. This note also serves as a supplement to our previous work [26].

[35] S. Pakdel, A. Rasmussen, A. Taghizadeh, M. Kruse, T. Olsen, and K. S. Thygesen, High-throughput computational stacking reveals emergent properties in natural van der Waals bilayers, Nat. Commun. **15**, 932 (2024).

[36] J. Li, M. Kuang, J. Bai, G. Ding, H. Yuan, C. Xie, W. Wang, and X. Wang, Coexistence of magnetic and phononic second-order topological phases in two-dimensional $NiZrCl_6$, Appl. Phys. Lett. **123**, 012201 (2023).

[37] N. Miao, B. Xu, L. Zhu, J. Zhou, and Z. Sun, 2D intrinsic ferromagnets from van der Waals antiferromagnets, J. Am. Chem. Soc. **140**, 2417 (2018).

[38] G. Kresse and J. Furthmüller, Efficiency of *ab-initio* total energy calculations for metals and semiconductors using a plane-wave basis set, Comput. Mater. Sci. **6**, 15 (1996).

[39] G. Kresse and J. Furthmüller, Efficient iterative schemes for *ab initio* total-energy calculations using a plane-wave basis set, Phys. Rev. B **54**, 11169 (1996).

[40] G. Kresse and D. Joubert, From ultrasoft pseudopotentials to the projector augmented-wave method, Phys. Rev. B **59**, 1758 (1999).

[41] J. P. Perdew, K. Burke, and M. Ernzerhof, Generalized gradient approximation made simple, Phys. Rev. Lett. **77**, 3865 (1996).

[42] S. L. Dudarev, G. A. Botton, S. Y. Savrasov, C. J. Humphreys, and A. P. Sutton, Electron-energy-loss spectra and the structural stability of nickel oxide: An LSDA+U study, Phys. Rev. B **57**, 1505 (1998).

[43] S. Grimme, S. Ehrlich, and L. Goerigk, Effect of the damping function in dispersion corrected density functional theory, J. Comput. Chem. **32**, 1456 (2011).